metals

MDPI

Article

The Effect of Co-Encapsulated GO-Cu Nanofillers on Mechanical Properties, Cell Response, and Antibacterial Activities of Mg-Zn Composite

Abbas Saberi [1], Hamid Reza Bakhsheshi-Rad [1,*], Ahmad Fauzi Ismail [2], Safian Sharif [3], Mahmood Razzaghi [1], Seeram Ramakrishna [4] and Filippo Berto [5,*]

[1] Advanced Materials Research Center, Department of Materials Engineering, Najafabad Branch, Islamic Azad University, Najafabad 57169-63896, Iran; abbassaberi65@gmail.com (A.S.); mahmood.razzaghi@gmail.com (M.R.)
[2] Advanced Membrane Technology Research Center (AMTEC), Universiti Teknologi Malaysia, Johor Bahru 81310, Malaysia; afauzi@utm.my
[3] Faculty of Engineering, Universiti Teknologi Malaysia, Johor Bahru 81310, Malaysia; safian@utm.my
[4] Department of Mechanical Engineering, National University of Singapore, 9 Engineering Drive 1, Singapore 117576, Singapore; seeram@nus.edu.sg
[5] Department of Mechanical and Industrial Engineering, Norwegian University of Science and Technology, 7491 Trondheim, Norway
* Correspondence: rezabakhsheshi@pmt.iaun.ac.ir (H.R.B.-R.); filippo.berto@ntnu.no (F.B.)

Abstract: Magnesium-based composites have recently been studied as biodegradable materials for preparing orthopedic implants. In this article, the graphene oxide (GO) and GO-Cu nanosystem has been homogenously dispersed as a reinforcement in the matrix of Mg-Zn (MZ) alloy using the semi powder metallurgy (SPM) method, and subsequently, the composite has been successfully manufactured using the spark plasma sintering (SPS) process. GO and GO-Cu reinforced composite displayed a higher compressive strength (~55%) than the unreinforced Mg-Zn sample. GO and GO-Cu dual nanofillers presented a synergistic effect on enhancing the effectiveness of load transfer and crack deflection in the Mg-based matrix. Besides, the GO-Cu dual nanofillers displayed a synergistic influence on antibacterial activity through combining the capturing influences of GO nanosheets with the killing influences of Cu. However, electrochemical and in-vitro immersion evaluation showed that Cu-GO reinforcement had a slightly negative effect on the corrosion behavior of the Mg-Zn sample, but the incorporation of GO enhanced corrosion resistance of the composite. Moreover, MZ/GO and MZ/GO-Cu nanocomposites showed acceptable cytotoxicity to MG-63 cells and revealed a high potential for use as an orthopedic implant material. Based on the research results, MZ/GO-Cu nanocomposite could be used in bone tissue engineering applications.

Keywords: magnesium; GO-Cu nanofillers; mechanical properties; corrosion resistance; antibacterial activity biocompatibility

Citation: Saberi, A.; Bakhsheshi-Rad, H.R.; Ismail, A.F.; Sharif, S.; Razzaghi, M.; Ramakrishna, S.; Berto, F. The Effect of Co-Encapsulated GO-Cu Nanofillers on Mechanical Properties, Cell Response, and Antibacterial Activities of Mg-Zn Composite. *Metals* **2022**, *12*, 207. https://cdoi.org/10.3390/met12020207

Academic Editors: Petra Maier and Leszek Adam Dobrzanski

Received: 19 November 2021
Accepted: 16 January 2022
Published: 22 January 2022

1. Introduction

Magnesium alloys have recently received much attention, and they are being recognized as a revolutionary range of biomedical materials [1]. Mg alloys have a density and elastic modulus comparable to natural human bone, which allows them to efficiently prevent the stress shielding effect [2,3]. Magnesium could be fully degraded in vivo and replaced by bone tissue without the need for additional surgery to remove the remaining parts [4,5]. Magnesium alloys show promise in orthopedic applications because of their outstanding properties [6,7]. Moreover, in physiological solutions, the degradation of magnesium-based implants generates a nontoxic soluble oxide that could be quickly excreted with no risk. Mg-based fixation implants, such as interference and maxillofacial plate screws, can be applied as biodegradable implants for non-load-bearing orthopedic

applications [8–10]. These devices are thought to provide adequate mechanical properties at the fracture site during new bone tissue healing before being replaced by natural tissue. Mg-based biomaterials have been the topic of comprehensive study over the last two decades [11–14]. However, the appropriateness of Mg alloys as a fracture fixation system has been questioned because of their low resistance to corrosion and relatively inferior mechanical properties. Different techniques have been utilized to resolve low corrosion resistance and insufficient yield strength of magnesium alloys, including preparation of Mg-based metal matrix composites (MMCs) using suitable bioactive reinforcements, which is steadily gaining interest [15–18]. Incorporating bio-metallic or bio-ceramic reinforcements to magnesium-based alloys to fabricate composites can improve biocompatibility, corrosion resistance, and mechanical properties. Using different reinforcements and adjusting their concentration could control the efficiency of the fabricated Mg-based MMCs [1,19]. To develop a novel Mg-based alloy with superior characteristics for clinical applications, Mg was alloyed with Al, Bi, Cu, RE, Zr, Mn, Ag, and Zn, among other elements. To minimize the corrosion rate of Mg, different Mg-based alloys were fabricated incorporating these elements. For example, Mg alloyed with Al and RE elements enhanced both corrosion resistance and mechanical strength [7,8,17,19]. However, Al has been proved to be toxic, and RE elements are quite costly. Unwarranted yttrium ions (Y^{3+}) changed the appearance of some rat genes and are thought to negatively influence DNA transcription factors. Liver, lung, nasopharyngeal, and breast cancers may be linked to other alloying metals such as zirconium (Zr) [1–3,7]. The incorporation of neodymium (Nd) and yttria (Y) to WE43 causes disruption of implantation site. Zinc is an essential component of the human body, as it is required for a variety of biological functions. Zn is known to promote age hardening response in materials by producing intermetallic compounds and refining grain size [7,15,16]. Due to the solution and precipitation strengthening, a little amount of Zn contributes to the strength [7,15–17]. Since zinc is more anodic to Fe and Ni, which may be present as impurities in Mg alloys, it aids in the prevention of corrosion. On the other hand, Zn and Mg share a hexagonal closed packed (HCP) crystal structure [1–3,7]. The possibility of employing zinc as an alloying element for Mg to produce biodegradable material was demonstrated in a recent study on the potential of Mg-Zn alloy.

It is important to note that the bacterial infections related to implants are increasing and should not be ignored [8]. The mentioned infections cause high medical costs and lead to higher suffering of patients. Mg alloys' relatively poor antibacterial activity can result in infections in the body, limiting their use in orthopedic applications [20]. Copper (Cu) and its compounds, because of the release of Cu ions, have high antibacterial activity [5]. Cu ions with a positive charge bind to the negative charge bacterial cell wall, disrupting membrane permeability and eventually cause bacteria death [21]. Besides, Cu ions may deactivate certain important enzymes by interfering with their thiol groups, resulting in bacterial cell death [22]. On the other hand, Cu is a crucial trace nutrition element for humans, acting as a catalytic cofactor for some essential metabolic enzymes [23]. In this respect, Mg alloy containing 0.25 wt.% of Cu fabricated by casting process was found to have antibacterial activity and excellent biocompatibility by Li et al. [24]. However, the investigations presented accelerated Mg degradation rates after alloying with Cu element, a problem that has yet to be resolved for Mg-Cu alloys applications [22]. As mentioned before, reinforcing and fabricating composites is a common way of improving the mechanical properties of Mg-based alloys. Mg-based composites have been fabricated with a range of carbon-based nanofillers, including carbon nanotubes and graphene. Particularly, graphene oxide (GO) performed admirably as a filler for Mg-based composites. The addition of just 1.5 wt.% of GO reinforcement resulted in a 358% increase in tensile strength, which can be attributed to the efficient filler-matrix interaction [25,26]. A variety of antibacterial agents, antibiotics, and nanofillers can also be integrated into Mg-based composites to improve their antibacterial properties [27]. Actually, only limited research has gone into developing new methods for improving the mechanical and antibacterial characteristics of Mg-based nanocomposite. The present investigation aims to see if adding Cu-GO dual

nanofillers to an Mg-based alloy during the fabrication process can improve its properties. For this purpose, the effects of reinforcing an Mg-based alloy biomaterial with GO-Cu on mechanical, corrosion, and biological properties were assessed. This study designed and incorporated co-dispersing GO-Cu nanofillers into an Mg-based matrix to enhance antibacterial action, cytocompatibility and improve mechanical properties.

2. Materials and Methods

2.1. Materials Preparation

Mg (99.5% purity, particle size less than10 μm), Zn (99.9% purity, particle size less than 3 μm), and Cu (99.5% purity, particle size less than 50 μm) powders were purchased from Merck Co. Mg, and Zn (with 3 wt.%) were mechanically alloyed in an argon atmosphere in a planetary ball mill, though confined in sealed 120 mL steel containers rotated at 300 rpm for 10 h. A combination of balls (Ø = 10 mm ball with 4.07 g mass and Ø = 20 mm ball with 32.65 g mass) was loaded into the container. The total weight of the powder in the vial was 12 g, with a ball-to-powder mass ratio of about 20:1. The SPM method was used to fabricate magnesium matrix reinforced with graphene oxide (GO) and Cu. In this regard, Mg-Zn was added as a matrix and mixed in ethanol for 1 h at 600 rpm by magnetic stirring. Cu (with 0.12, and 0.25 wt.%) powders were mixed in ethanol using a mechanical agitator. At the same time, 0.5 wt.% GO nano-platelets for 3 h were separately ultrasonicated in ethanol. GO solution (with 0.5 wt.%) was added drop wise into the above magnesium alloy and Cu powder solution in ethanol. The mixing process continued for 1 h to obtain a uniform mixture. The mechanically agitated blend was filtered, and the vacuum dried overnight at 70 °C to achieve the composite powder. To acquire green billets with dimensions of $\phi 10 \times 10$ mm^2, the composite powders wherein Mg-Zn-0.5wt.%GO-xCu (x = 0.12, and 0.25 wt.%) have been labeled as MZ, GC1, and GC2, respectively. The composite powders were sintered at the temperature of 570 °C, the pressure of 40 MPa, and holding times of 10 min in a spark plasma sintering (SPS) chamber, as shown in Figure 1.

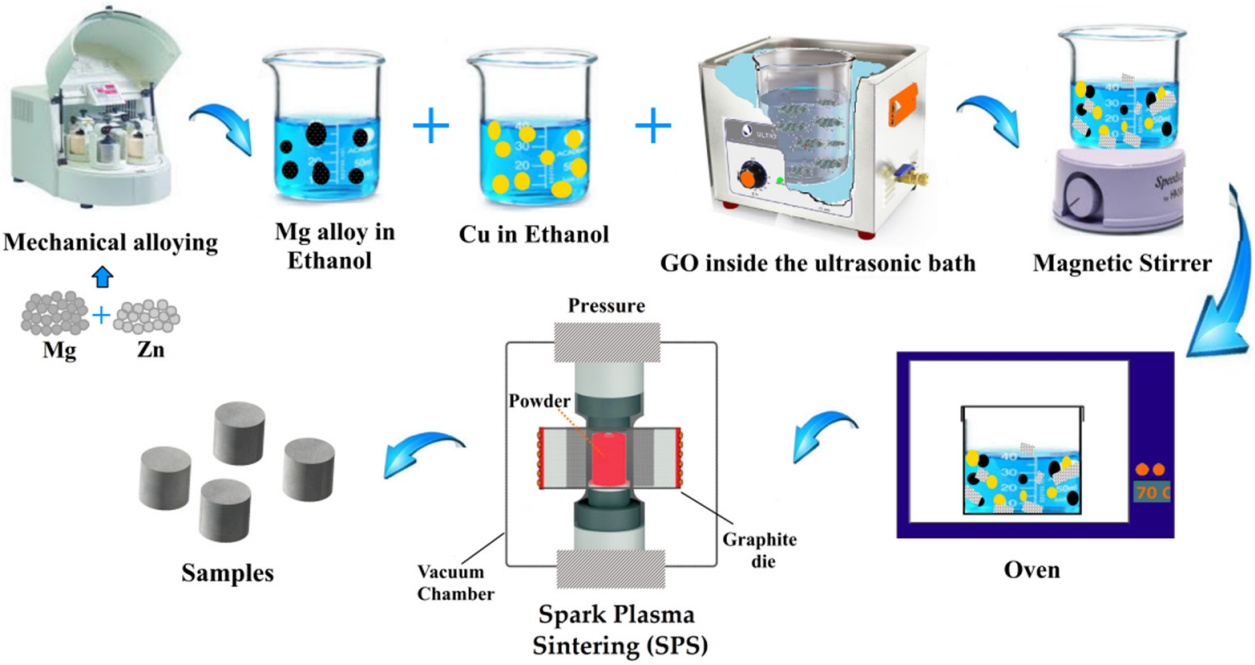

Figure 1. Illustration of the process of MZ/GO-Cu composite preparation using semi powder metallurgy and spark plasma sintering (SPS) methods.

2.2. Microstructure and Mechanical Properties

Field emission scanning electron microscope (FESEM, Tescan, Mira 3 Czech Republic) equipped with energy dispersive spectroscopy (EDS, JSM-5910LV, JOEL Ltd., Tokyo, Japan) and transmission electron microscopy (TEM; H-800, Hitachi, Tokyo, Japan) were utilized to

investigate the composition distribution and more detailed evaluations of microstructure. An X-ray diffractometer (XRD, D8 Advance, Brucker, Karlsruhe, Germany) was used to detect constituent phases. Cu-Kα of X-ray and a scanned velocity of 8° min^{-1} were the experimental conditions for XRD. The surface water contact angles were determined by using the sessile drop method in the air at room temperature using a video contact angle instrument (Dataphysics OCA 15, DataPhysics Instruments GmbH, Filderstadt, Germany) to determine the wettability of the matrix and nanocomposites surface with a drop size of 10 mL. The results of three samples were used to determine the average contact angle of each type of material. The compressive strength of the cylindrical composites (diameter = 10 mm, height = 15 mm) with GO and different percentages of GO-Cu was measured by pressing them at room temperature with the SANTAM universal testing machine at a speed of 2 mm/min and a load of 10 KN (ASTM-E9 standard). Furthermore, a Vickers hardness tester (HMV-2T E, Shimadzu, Kyoto, Japan) with 300 g force was used to determine the microhardness of the samples.

2.3. Corrosion Behavior

To assess the corrosion rate, an EC-Lab system was used to conduct a potentiometric polarization test in the SBF solution at a voltage range of –250 to +250 mV SCE an open circuit potential at a rate of 0.5 mV per second. The specimens were examined with a specific surface of 1 cm^2 exposed to the electrolyte as the working electrode, a graphite electrode as the counter electrode, and a saturated calomel electrode (SCE) as the reference electrode. The corrosion potential, the density of current corrosion, and the slope of the anodic and cathode curves were all determined using the EC-Lab express software. After 30 min of sample placement in the SBF, electrochemical impedance spectrometry (EIS) was used to achieve potential stability. The ASTM G106 standard was used to conduct this test at an open circuit potential and in the frequency range of 10^5 to 10^{-2} Hz, with a sine signal with a potential amplitude of 10 mV. The samples were immersed in 200 mL of Kokubo SBF solution, with a pH of 7.4, for the immersion test, according to ASTM G1-03 standard. After each 24 h period during the immersion test, the value and difference in the SBF solution's pH value were measured. The mass loss experiments for the composites were carried out in accordance with ASTM standard G31-72. The cleaned composites with a diameter of 10mm and a height of 5mm were weighted and soaked in SBF at 37 °C for 24 to 144 h. The surface corrosion products of composites were cleaned with chromic acid solution (300 g/L Cr_2O_3 + 10 g/L $AgNO_3$) before weight loss measurements. To achieve repeatable findings, each test was repeated three times. A pH meter was used to test the pH of the solution during processing. In addition, according to Ref [20], the volume of H_2 released as a result of the magnesium dissolution was calculated. After immersing the composites in SBF and funneling them, a burette filled with SBF was placed upside-down directly above them to trap the H_2 gas and measure the volume of H_2 released.

2.4. Antibacterial Activity

The antibacterial behavior of the specimens against gram-negative bacteria (*E. coli*) and gram-positive bacteria (*S. aureus*) was assessed employing the disc diffusion method to study the biological activity of each MZ/GO and MZ/GO-Cu composites. For this purpose, the cultivation environments were lawns, and the sterile swabs dipped in the microbial suspension were flushed by pressing swabs to the side of the pipe. The composites were incubated in an agar medium for 24 h at 37 °C. The inhibition area (IA) around the samples showed their antibacterial behavior. A broth culture medium was also used for culture forming unit (CFU) testing. To make a microbial suspension, between 3 and 4 pure colonies of *E. coli* and *S. aureus* from a 24 h culture were extracted by loop and applied to the broth solution, then vortexed for 24 h before being put in the incubator. The opacity of the solution was then increased to 0.8, and then the prepared specimens were exposed to the bacterial broth solution for 24 h.

2.5. In-Vitro Biocompatibility

The in vitro cytotoxicity of the MZ/GO and MZ/GO-Cu composites was determined using an indirect 3-(4,5-dimethylthiazol-2-yl)-2,5-diphenyltetrazolium-bromide (MTT, Sigma, Saint Louis, USA) assay, based on the extraction technique. The amount of 5 mg of each nanocomposite was applied to the culture medium and incubated for 1 and 3 days at 37 °C. The cell medium was refreshed with 1- and 3-day extracts after 10^4 cells/mL were refined on the 96-well plates for 24 h. After another 24 h, the medium was removed, and 100 mL of MTT agent (0.5 mg/mL in PBS) were inoculated into each well and held in the incubator for 4 h. After 4 h, 100 µL of Dimethyl sulfoxide (DMSO) was pumped into the well to dissolve the formazan crystals. Lastly, the absorbance was measured at 545 nm using an ELISA Reader (Stat Fax-2100, Miami, FL, USA) and compared to a control group of free nanocomposites culture medium. Nuclear staining with DAPI (40, 6-diamidino-2-phenylindole, blue fluorescence in live cells) was used to investigate MG63 cell proliferation on the composites under fluorescence microscopy.

2.6. Statistical Analysis

The experimental data outcomes assessed via the program SPSS 19.0 and presented based on the average ± standard deviation. Student t-tests were performed be-tween various groups to evaluate p values that were assumed to be significant when $p < 0.05$ was employed.

3. Results and Discussion

3.1. Microstructure

Figure 2 depicts the SEM micrographs of the morphologies of pure Mg, pure Zn, pure GO, nano-Cu, and MZ/GO-Cu mixed powders (Figure 2a–d). The preliminary powder particle sizes of Mg and Zn were various in order to achieve a homogeneous distribution of other alloying elements in Mg. Milled Mg powders have shown a lamellar structure and a larger surface area due to severe plastic deformation and cold welding of Mg particles. The effective contact area between the particles increases, allowing for easier sintering densification [1]. Figure 2e,f shows the original GO with clearly flaky, with comparatively smooth surfaces and sharp edges. It should be mentioned that the GO surface has many wrinkles. Furthermore, as could be seen in figures, the GO sheets were interconnected to form micro-space network structures in the particles; but the Cu particles had dendritic shape particles (Figure 2g,h). The MZ/GO-Cu mixed powders surface had several tiny wrinkles, as shown in the high magnification image in Figure 2i,j, and its edges become smoother. The images also showed a consistent distribution of Cu inside the GO sheet and strong attachment and anchoring.

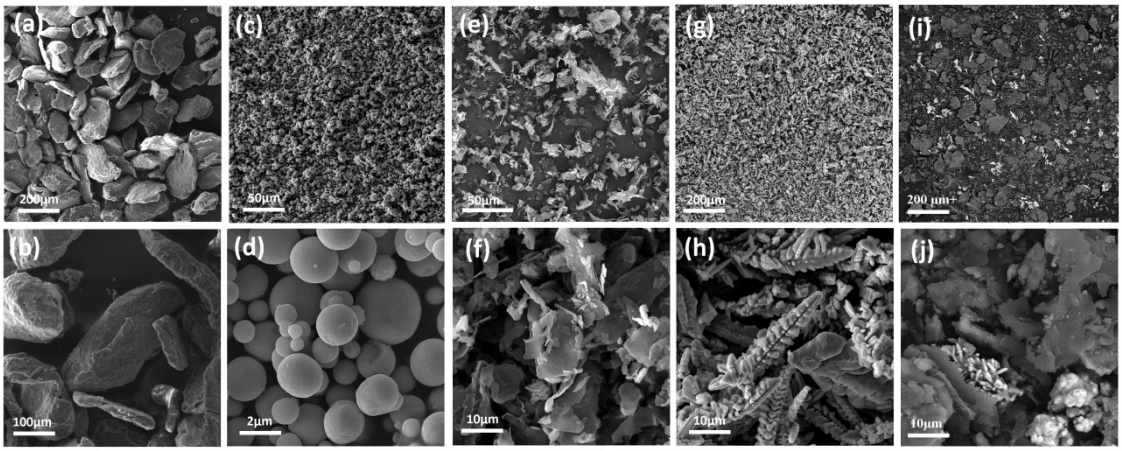

Figure 2. SEM micrographs of (**a**,**b**) Mg, (**c**,**d**) Zn, (**e**,**f**) GO, (**g**,**h**) Cu and (**i**,**j**) MZ/Cu-GO powders.

Figure 3a,b depicts the TEM images of Mg and GO. The TEM images revealed that the GO powders were made up of nanosheets with thicknesses of a few nanometers and sizes varying from a few to hundreds of microns, as shown in Figure 3b. Moreover, Figure 3c,d shows the Cu nanoparticles with spherical morphology. The complex structure of the MZ/GO and MZ/GO-Cu composite was also evident in the TEM images, as shown in Figure 3e–h. The surface of GO nanosheets was smooth and had wrinkled layer morphology. On the other hand, multiple spherical-like Mg and Cu nanoparticles were observed on the entire GO surface in the MZ/GO-Cu mixed powders. Moreover, it was observed that the interaction between the Cu and GO was strong because nearly all of the Cu particles were attached on the surface of GO, and very few Cu particles resided outside the GO support.

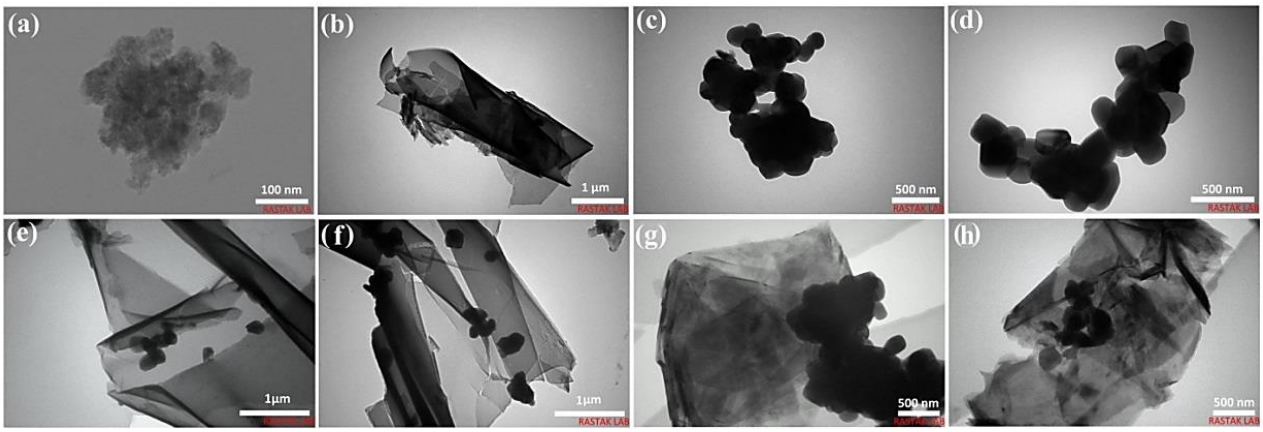

Figure 3. TEM micrographs of (**a**) Mg, (**b**) GO, (**c**,**d**) Cu, (**e**,**f**) MZ/GO (G), (**g**,**h**) MZ/GO-Cu powders.

Figure 4 depicts the EDS mapping of Mg, Zn, GO, and Cu. The existence and distribution of GO and Cu inside Mg-based matrix is shown by the EDS analysis. The EDS analysis is confirmed the presence of Zn, Cu, O, and C in the Mg-based matrix composite. Individual GO nanoplatelets were decorated on the surface of the Mg alloy particles when the pre-dispersion was completed. It is an ideal dispersion of GO nanoplatelets and Cu in this stage which has a significant impact on the mechanical property of the composite.

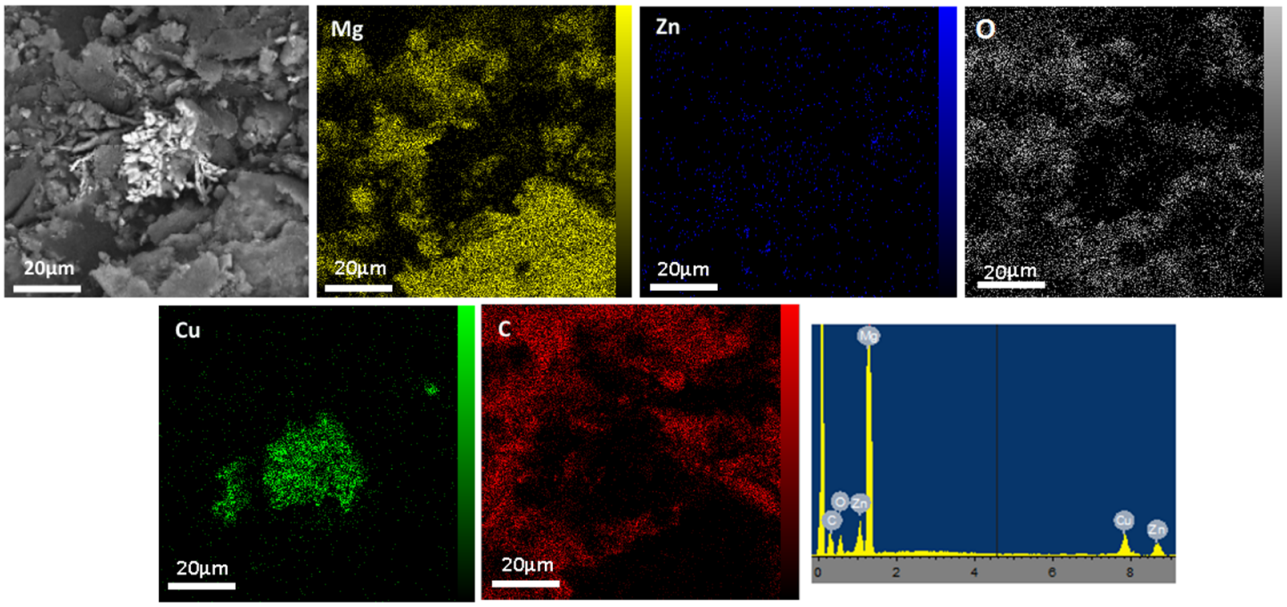

Figure 4. SEM, EDX, and map images of MZ/2GO-Cu powder composites.

XRD analysis was used to better classify the phases in the Mg-based composite composites, which the findings are depicted in Figure 5a. Only one set of well-defined peaks for α-Mg was found in pure Mg, and no peaks for second phases were found [28]. One can confirm the crystalline nature of the as-prepared graphene sample by observing the peak in the XRD pattern. Additionally, the XRD pattern of Zn and Cu was found in the pure sample, while no peaks for the second phases were found. The combined diffraction peaks corresponding to the α-Mg matrix, $MgZn_2$, and MgZnCu phases [21] were visible in the MZ/GO-Cu composite XRD pattern. In the complete persistent XRD pattern of the MZ/2GO-Cu composite, the graphene (001) peak [20] was not clearly noticeable. This may be due to the separation of graphene multilayers into monolayers (by splitting van der Waals bonds) in the solution. In addition, the samples having a much lower concentration of graphene, which is beyond the detection limit of XRD analysis.

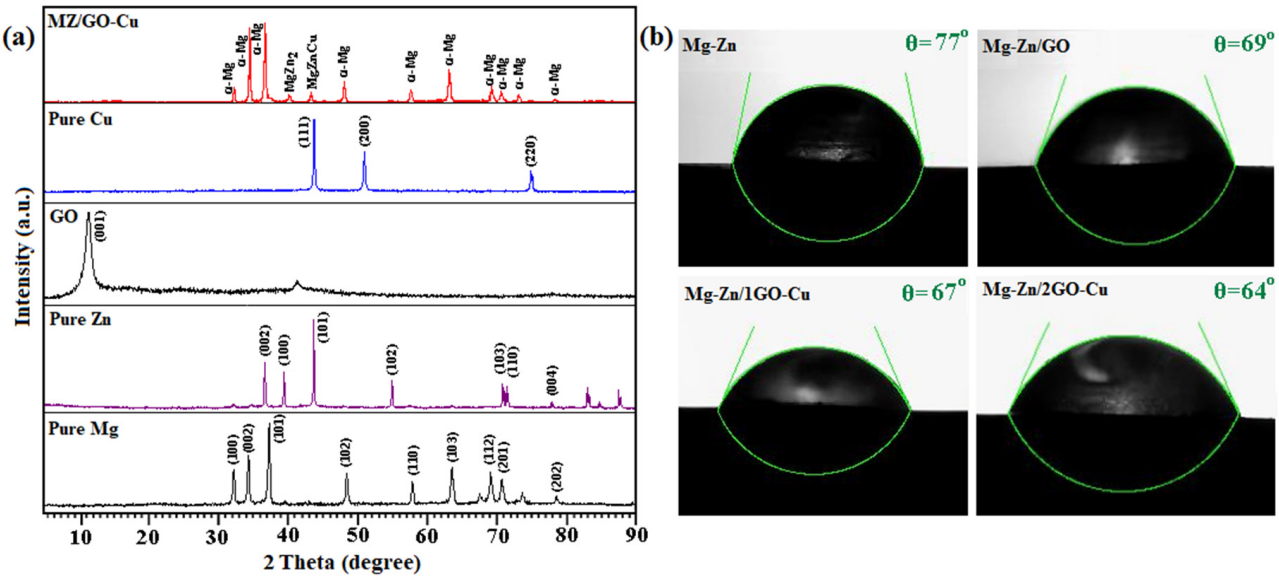

Figure 5. (**a**) XRD pattern and (**b**) Contact angle of MZ, MZ/GO, MZ/1GO-Cu and MZ/2GO-Cu composites after SPS process.

Figure 5b shows the water contact angles determined by surface water droplet deposition. The water contact angle of MZ alloy was 77 ± 1.23° while the water contact angles for MZ/GO, MZ/1GO-Cu, and MZ/2GO-Cu composites were decreased to 69 ± 2.20° and 67 ± 1.10° and 64 ± 1.20°, respectively, suggesting that GO and GO-Cu nanofillers improved the surface hydrophilicity of MZ/GO composites. This behavior can be attributed to the presence of functional groups (carboxyl group, carbonyl group, and hydroxyl group) at the edges of GO leads to the hydrophilicity of the composite [4,29]. The integrated GO-Cu nanofillers were orderly exposed to the surface in MZ/GO-Cu composites, resulting in a significant change in surface micro-texture and chemical composition. In particular, the exposed Cu-GO nanosized reinforcement was capable of attracting water molecules via hydrogen bonding, promoting water penetration into the Mg-based matrix. The embedded GO-Cu particles were exposed to the surface in an organized manner in the MZ/GO-Cu composite, resulting in a significant improvement in the surface microtexture. These findings may be clarified by the hydrophilic existence of GO, which includes a large number of hydroxyl functional groups [27]. The increased surface hydrophilicity of the bone- implant was thought to be beneficial for absorbing nutrient substances and bioactive factors, thereby speeding up bone healing when implanted in vivo.

3.2. Mechanical Properties

In clinical applications, a biomedical material's mechanical properties are very important. As a result of the limited specimen size, the hardness and compressive strength were

only evaluated. The microhardness of MZ matrix was increased by adding Cu and GO nanosheets (Figure 6a). The hardness of MZ, MZ/GO, MZ/1GO-Cu, and MZ/2GO-Cu was 64 ± 2.1 HV, 75 ± 3.7 HV, 86 ± 3.9 HV, and 91 ± 4.7 HV, respectively. The MZ/2GO-Cu composite has the highest hardness, which is significantly higher than that of MZ. Overall, adding GO to the Mg-based matrix enhanced mechanical properties through synergetic strengthening mechanisms such as grain refinement (GR) and load transfer (LT) strengthening as well as geometric mismatch (GM) between Mg particles and GO fillers [30]. By providing a pinning effect on the grain boundaries of the Mg matrix, the addition of Cu and GO reinforcement phase particles to MZ inhibits grain growth and hence the increased hardness of the composite [31].

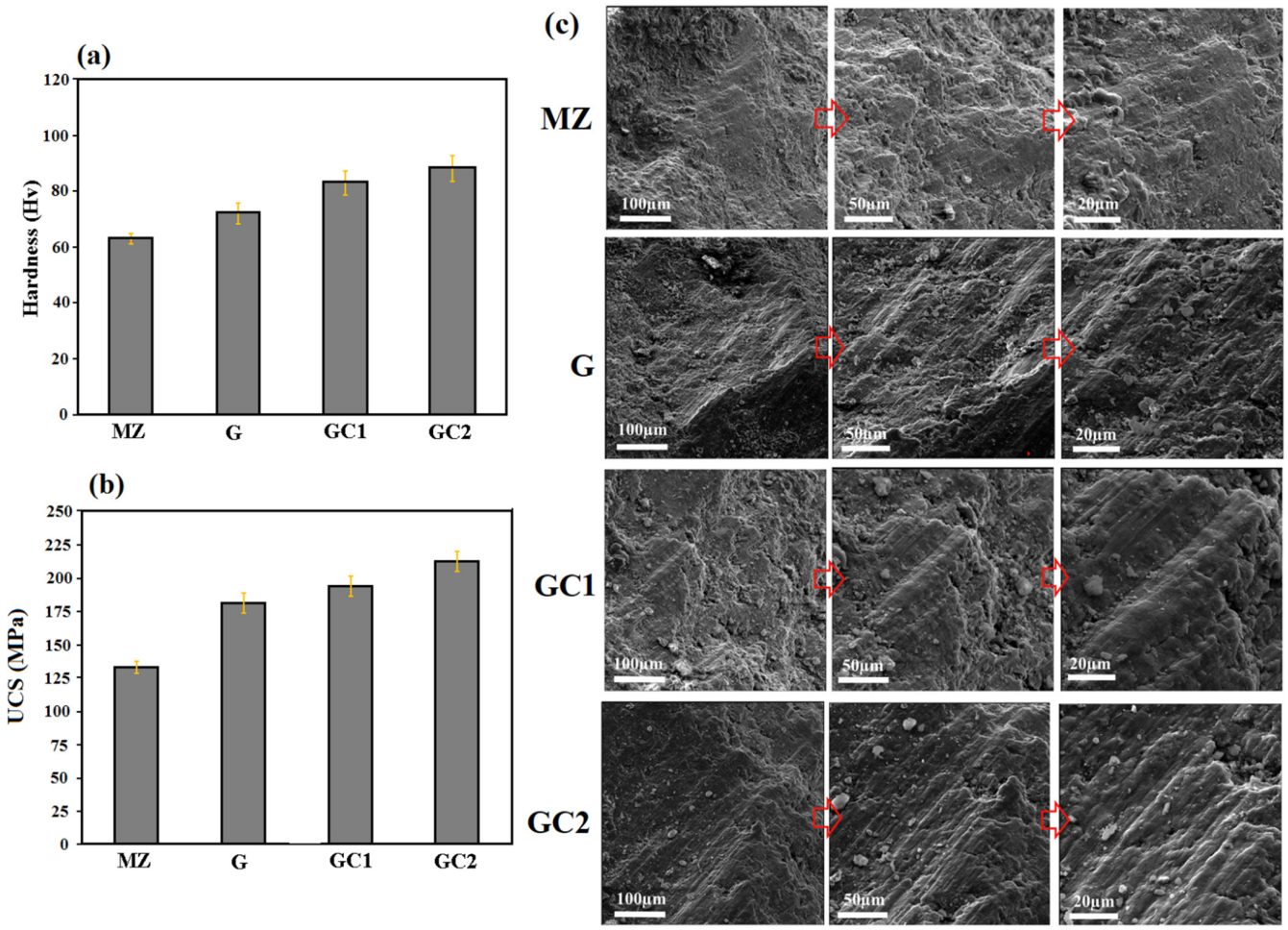

Figure 6. (**a**) Microhardness value, (**b**) Ultimate compressive strength (UCS) value of MZ, MZ/GO (G), MZ/1GO-Cu (GC1), and MZ/2GO-Cu (GC2) composites, and (**c**) SEM images of fracture surfaces of MZ, MZ/GO (G), MZ/1GO-Cu (GC1), and MZ/2GO-Cu (GC2) composites after compression testing.

The compressive strength test was performed to assess the effects of the phase of reinforcement on the biocomposites' mechanical properties. The compressive strength value of MZ, MZ/GO, MZ/1GO-Cu, and MZ/2GO-Cu composites is presented in Figure 6b. As can be observed, using dual nanofillers (GO and Cu) will improve the mechanical properties of MZ-based composites. The mechanical strengthening effects of GO and Cu on Mg-based composites are interestingly distinct. The MZ/2GO-Cu composite had the highest UTS, which could be because of the transfer of load from the Mg-based matrix to the GO reinforcements with much higher Young's modulus (E_{GNPs} = 1 TPa) through the Mg/GO interfaces [19]. The interfacial attachment of the reinforcing particles with the

underlying metal matrices is important for the load transfer from the Mg-based matrix to the reinforcing particles [32]. The homogenous distribution of GO as reinforcement particles in the Mg-based matrix can efficiently load-transfer from the matrix to the GO during the applied load, resulting in enhanced load-bearing ability and increased strength of the matrix. This could be attributed to the presence of distributed GO and Cu in the Mg-based matrix creating steric obstacles to dislocation in the MZ/GO-Cu composite during compressive load, raising deformation resistance [33].

Figure 6c depicts the SEM morphologies of compressive fracture surfaces of MZ/GO-Cu nanocomposites. All of the specimens exhibited fracture at an angle of approximately 45° to the loading axis of the compression. Several cleavage properties of MZ/GO-Cu nanocomposites were observed, all consistent with a standard brittle fracture pattern. The deformation behavior of Mg-based composites is controlled by twinning shear bands. As a result of shear band deformation, work-hardening behavior and heterogeneous deformation are attributed to the shear bands [19,33]. Work-hardening rates are higher for samples that fail due to shear band deformation. This type of shear band is reported [8] to be common on Mg's compressive fracture surfaces and suggests the dominance of tensile twinning as the dominant plastic deformation mode when the material is subjected to compressive load. An additional obstacle to dislocation slip propagation and dominating tensile twin propagation in the Mg-based matrix was provided by Cu and Go in the Mg-based matrix [8,33]. This was particularly true at the magnesium interparticle boundaries. The increase in shear band spacing observed on the fracture surfaces of MZ/GO-Cu composites can be attributed to the significantly more ductile compressive fracture behavior of nanocomposite containing a moderate amount of Cu and GO.

3.3. Corrosion Properties

Figure 7a illustrates the pH variations of MZ, MZ/GO, and MZ/GO-Cu composites during immersion in SBF solution. The pH values of all MZ/GO-Cu composites rise quickly in the first 20 h, then steadily increased with raising immersion time. After 140 h of immersion, the pH of the composite containing Cu was higher than that of the MZ and MZ/GO composites, which may be attributed to the fact that the MZ and MZ/GO composites had a smaller galvanic cell than the composite containing Cu, resulting in accelerated deterioration of the Mg-based composite comprising high concentrations of Cu [21,22]. The pH values of MZ/GO-Cu composites were still higher than those of MZ alloy during the immersion test, suggesting that applying a large volume of Cu to the MZ/GO matrix accelerates the degradation rate. Figure 7b shows the plots of H_2 evolution against immersion time for MZ and MZ/GO-Cu composites specimens in SBF solution. The MZ and MZ/GO composites had the lowest H_2 evolution in comparison with the MZ/GO-Cu composites. The observation revealed that the hydrogen evolution had a comparable trend of increment for all of the samples. Nevertheless, this increasing rate was reduced with increasing the time of immersion. The reason for this change could be due to the precipitation of insoluble corrosion products on the surface. Based on the results, the MZ and MZ/GO composites displayed the lowest, and the MZ/GO-Cu composite displayed the highest hydrogen evolution rates. The rate of degradation was increased with a further increase in Cu content from 0.12 to 0.25 wt.%, which could be because of the major role of Cu in the formation of the galvanic cell on the alloy.

The polarization curves attained from the electrochemical measurements of the MZ, MZ/GO, and MZ/GO-Cu composites are depicted in Figure 7c. The corrosion current density of MZ (187 ± 5 $\mu A \cdot cm^{-2}$) and MZ/GO-Cu composites rapidly increased from 210 ± 8 to 384 ± 12 $\mu A \cdot cm^{-2}$ with Cu loading rising from 0.12 to 0.25 wt.%. However, the magnesium composite containing GO presented the lowest corrosion current density (126 ± 4 $\mu A \cdot cm^{-2}$). The EIS test for the MZ/GO-Cu composites in the SBF was carried out to validate the polarization result. GO-Cu incorporation decreased the sizes of the capacitive loops in the MZ/GO-Cu composite, meaning that GO-Cu addition can negatively affect the corrosion resistance. The impedance decreased for the GO-Cu concentration of

upper than 0.12 wt.% because of the clustering of GO-Cu nanoparticles. As a consequence, the impedance of the MZ/GO composite was the largest, suggesting that the composite encapsulated with GO has the highest resistance to corrosion. The electrical elements mentioned in the circuits introduced in Figure 7d were utilized to fit the experimental results, where Rs is the electrolyte resistance between the working and reference electrodes, Rct is the charge transfer resistance, and CPE-dl is the electric double-layer capacitance of the passive film. According to the outcomes, MZ/GO had a higher Rct value (G; 182.3 $\Omega.cm^2$) than MZ/1GO-Cu (128.2 $\Omega.cm^2$) and MZ/1GO-Cu (99.6 $\Omega.cm^2$), which is strongly in-line with the polarization test results. The higher Rct value of MZ/GO composite is related to the presence of graphene, since it is a natural diffusion barrier that protects the Mg matrix against corrosion because it has good chemical inertness and impermeability to molecules. Thus, it delayed the invading of the corrosion medium and hence the corrosion of Mg alloy. However, in MZ/1GO-Cu composite, GO-Cu nearly encapsulated the Mg alloy grains, and the occurrence of galvanic corrosion leads to acceleration of the corrosion of Mg alloy and revealing a strong corrosion rate [28]. Recent studies indicated that a single atomic layer of GO consisting of sp2-C bonds is impermeable to gas molecules and established an atomic-scale barrier that prevents even helium gas from passing through it [33]. On the other hand, the corrosion of Mg alloy became anabatic when the Cu content was introduced to MZ/GO composite, which could be because of the formation of a galvanic cell between the matrix and reinforcement phases [15]. Thus, co-incorporation of GO and Cu in the matrix of magnesium has a reversed effect on the corrosion behavior of the alloy.

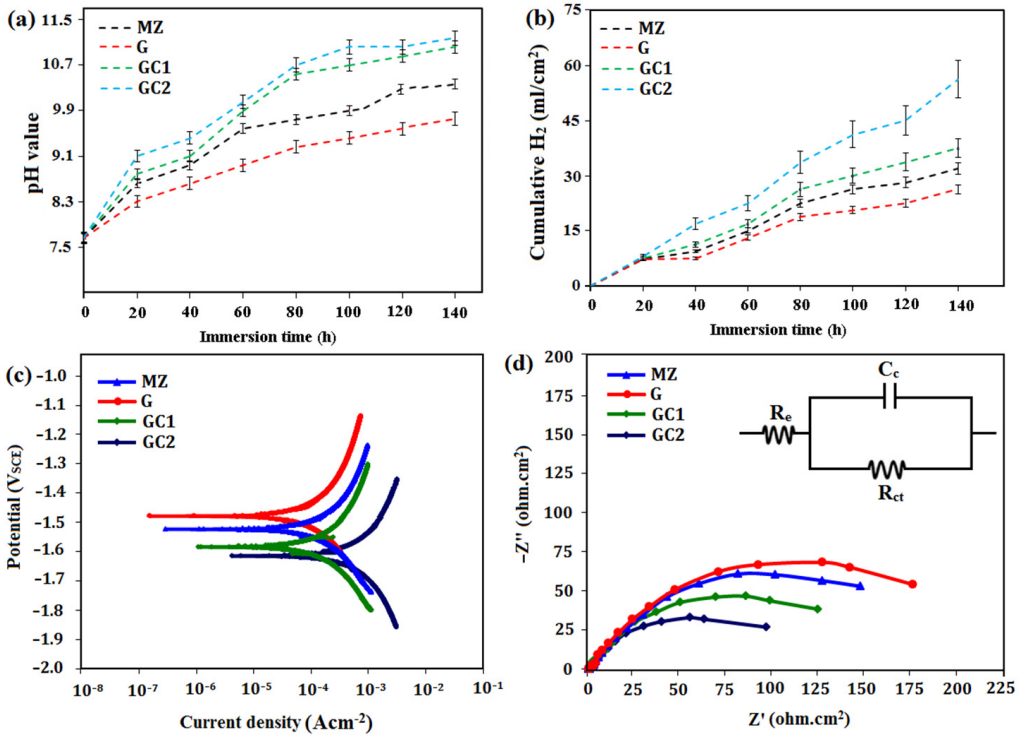

Figure 7. (**a**) pH value, (**b**) H_2 evolution, (**c**) Potentiodynamic polarization curves, and (**d**) Nyquist plots of MZ, MZ/GO (G), MZ/1GO-Cu (GC1), and MZ/2GO-Cu (GC2) composites. Note: Image in the frame is the equivalent circuit used to model the results of Mg-based composite.

The degradation behavior of the MZ/GO-Cu composite was investigated using immersion testing, as seen in Figure 8a–d. With the soaking time lengthening, all of the MZ/GO-Cu composites showed corrosion attack. However, the MZ/2GO-Cu composite undergoes more corrosion attacks than the MZ/1GO-Cu, meaning that the added Cu accelerates the rate of deterioration. The increased galvanic cell area, induced by adding Cu, enhanced the degradation rate of MZ/GO-Cu composites. In addition, for the MZ/1GO-Cu

and MZ/2GO-Cu specimens, pitting corrosion was detected, which resulted in the forming of corrosion cracks with a dense corrosion product layer. While the MZ and MZ/GO composite had thin cracks and smaller corrosion pits. It is worth noting that just a few corrosion pits were developed on the composite without Cu compared to the composite with Cu. Overall, the EIS findings were consistent with the PDP and in vitro immersion results. The illustration of the corrosion mechanism of the MZ/GO-Cu composites is depicted in Figure 8e to explain the increased corrosion resistance. The most common form of corrosion in the MZ/GO-Cu alloy is galvanic corrosion between the intermetallic phases and the Mg-based matrix. The surface of the Mg-based matrix then develops a layer of corrosion products as a result of the reactions mentioned below:

$$Mg + 2H_2O \longrightarrow Mg(OH)_2 + H_2 \quad (1)$$

The corrosive medium can begin to corrode the Mg-based matrix as the process continues, as can be seen in Figure 8e. Mg alloy is infiltrated by the corrosive medium and corrodes at the initial stage. The corrosive medium further penetrated the reinforcement process for MZ/GO, and MZ/GO-Cu composite with GO encapsulated Mg matrix. As a consequence, the GO plate encapsulation was able to retain its structural stability and fill the Mg-based porosity more reliably and strongly. In addition, GO by blocking the ionic transport (chloride ion) into the Mg matrix through the incorporation of GO into the Mg matrix reduces the infiltration of the electrolyte to the surface of Mg alloy and builds an obstacle for blocking the ionic transport in the Mg matrix [34]. As a result, the corrosive medium's penetration into the fresh Mg matrix may be slowed down [35]. However, the addition of Cu into the MZ/GO composite increases the corrosion rate, indicating that Cu addition adversely affected the corrosion resistance due to the occurrence of severe galvanic corrosion in the secondary phase containing Cu/Mg system. Figure 8f shows the XRD pattern of the MZ/GO-Cu after 7 days of immersion in SBF. It can be seen that the corrosion products are $Mg(OH)_2$ and HA, which is a result of the existence of inorganic ions such as $H_2PO_4^-$, Cl^-, and Ca^{2+} in the SBF solution [5].

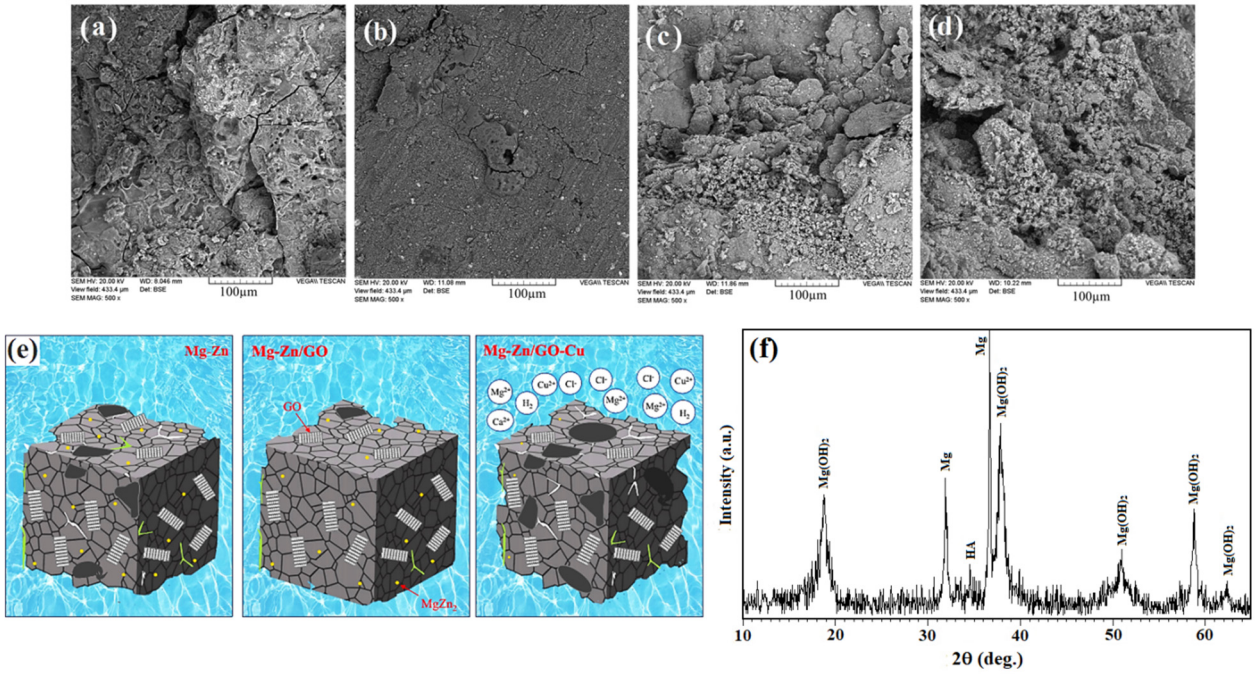

Figure 8. SEM images of the samples (**a**) MZ, (**b**) MZ/GO (G), (**c**) MZ/1GO-Cu, and (**d**) MZ/2GO-Cu composites after immersion in SBF solution for 7 days and (**e**) schematic model for corrosion process of MZ, MZ/GO, and MZ/2GO-Cu composites, (**f**) X-ray diffraction patterns of MZ/GO-Cu after soaking in SBF for 7 days.

3.4. Cell Response

After being inserted into the body, the biodegradable implant will react with the surrounding body fluid and ultimately degrade when tissue is completely healed. Figure 9a–d shows the fluorescent microscopic images of MZ, MZ/GO, MZ/1GO-Cu composites where MG-63 cell lines were cultured. After 2 days of culture, the MZ and MZ/GO composite had slightly more cells than the MZ/GO-Cu composites. The DAPI nuclei staining showed that the MG-63 cells had adequate interactions between adjacent cells on MZ/GO-Cu composite and presented osteoblast cells attachment and proliferation accommodated by the composite containing a low concentration of Cu (except for the GC2 composite).

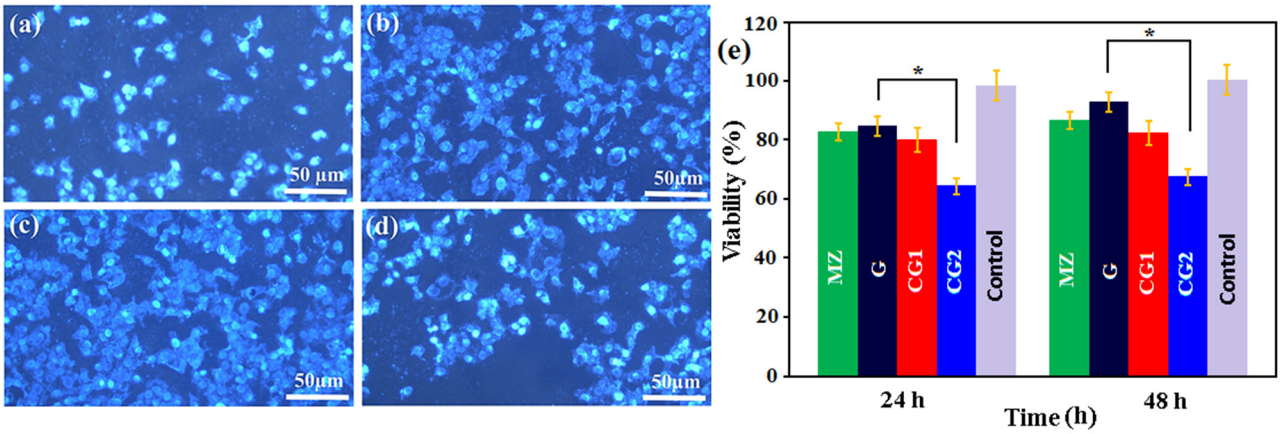

Figure 9. Fluorescent microscopic images of (**a**) MZ, (**b**) MZ/GO (G), (**c**) MZ/1GO-Cu (GC1), (**d**) MZ/2GO-Cu (GC2), and (**e**) cell viability of MG63cells cultured for 24 and 48 h on MZ/GO-Cu composites (* $p < 0.05$).

An MTT assay experiment was used to determine cell viability quantitatively, with the findings depicted in Figure 9e. Cell viability on MZ and MZ/GO composites clearly improved with increasing the incubation time. The cell viability values for the MZ alloy improved from 82 to 91% after 96 h of culture, while the GC1 composite does not change almost 80 to 82%. More specifically, at the same culture period, MZ/GO showed higher cell activity (96%) than composite with higher Cu (70%), implying that a high concentration of Cu inhibited cell proliferation. The outcomes showed that adding GO to the MZ alloy can improve the cell response. The improved cell response can be attributed to slower corrosion and ion release, as well as a pH rise, which was thought to have a significant impact on cell growth [28,34]. Furthermore, the addition of a low amount of Cu has been extensively studied and noted for its osteostimulatory and angiogenic properties, implying that it could be useful in healing bone damage caused by infection [22,24]. Overall, the MZ/GO composite and the composite with a low Cu concentration induce less toxicity and greater implant/bone-bonding, and quicker bone maturation [21]; this may be because of the release of bioactive ions during the degradation process. Mg is also vital for the formation of biological apatite and bone metabolism, and a lack of it may result in inadequate bone growth and increased resorption. On the other hand, Cu in low concentration is needed for the physiological processes of bone cells, and a deficiency in Cu may contribute to osteoporosis and other diseases. Cu has the potential to affect bone metabolism, such as bone resorption. With the Bsp and Cola1 in the ECM, trace amounts of Mg and Cu can serve as co-factors influencing the bone mineralization method [21,22,24]. The stimulatory effect of GO on cell performance might be because of its surface oxygen-containing functional groups [36]. It was reported [37] that the hydroxyl groups on GO could offer sites for maintaining and getting cells onto the fibrous, improving cell adhesion. Similarly, it is suggested [4,38] that GO offers a platform to create a bio-interface for cell proliferation and growth. As a result, the low concentration of GO-Cu resulted in lower toxicity, which was

advantageous for osteoblast cell proliferation and differentiation, whereas the composite's positive barrier property may also mitigate the negative effects of rapid corrosion.

3.5. Antibacterial Activity

Figure 10a show the inhibition area (IA) of the MZ alloy and MZ/GO-Cu composites, indicating qualitatively evaluated antibacterial activity after 24 h. As predicted, the MZ alloy has a lower antibacterial activity. The IA diameter of the GC1 composite was 2.34 mm, while the diameter of the MZ alloy was 0.1 mm. It is worth mentioning that the GC2 composite has a greater IA diameter (3.64 mm) than the other composites against *E. coli*. Similarly, the inhibition zone diameter of MZ, G, GC1, and GC2 composites was in the range of 0.1 mm, 2.47, 3.51, and 4.03 mm against gram-positive (*S. aureus*), suggesting that GO and Cu had a synergistic impact on the antibacterial efficiency of the MZ-based composite. By raising the Cu contents from 0.08 to 0.25 wt.%, the inhibition zone increased to 2.47 and 4.03 mm, respectively, against gram-positive (*S. aureus*). This could be because of the high release of Cu ions from MZ/2GO-Cu composites.

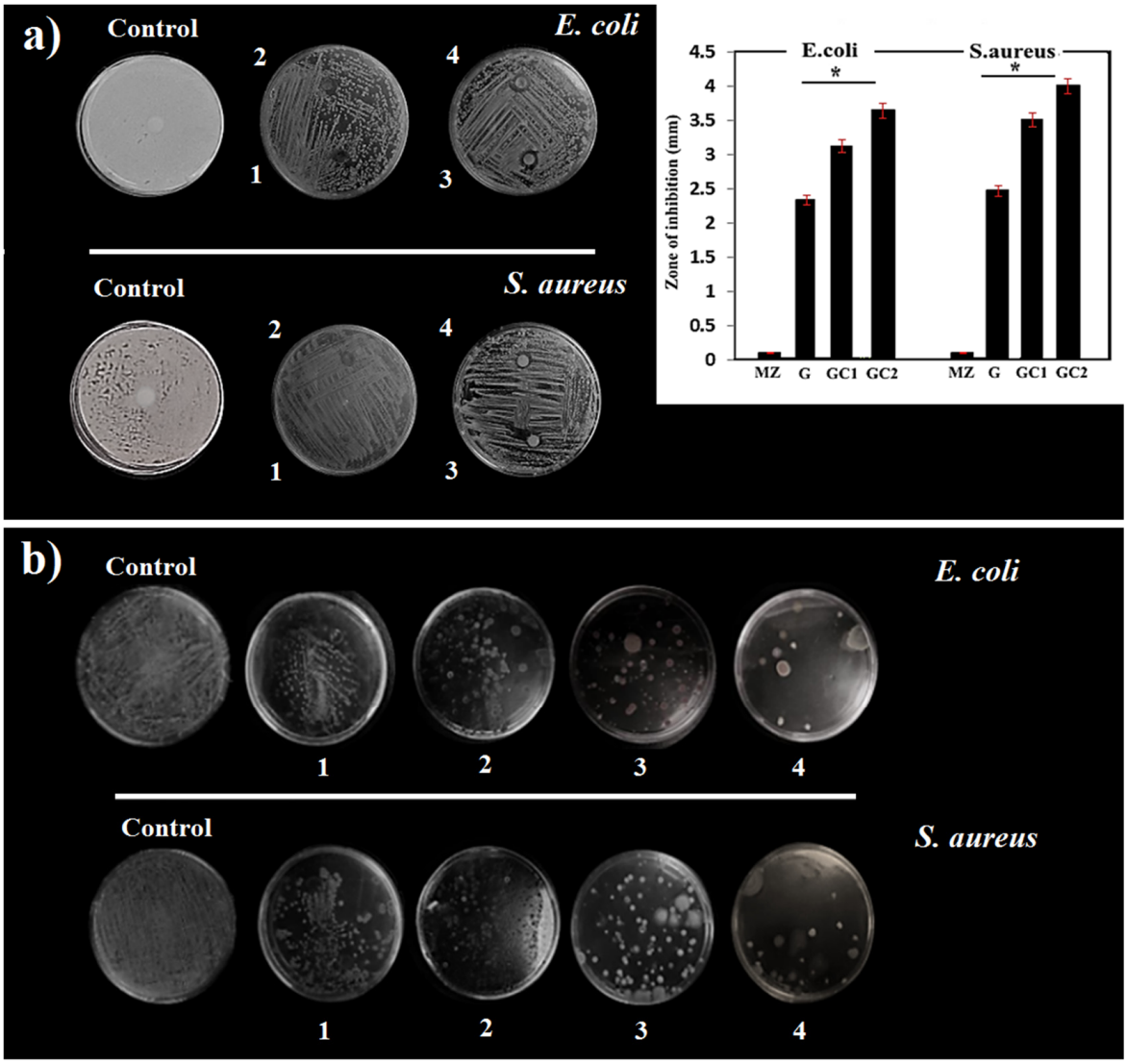

Figure 10. (**a**) Antibacterial activities of the (1) MZ, (2) MZ/GO (G), (3) MZ/1GO-Cu (GC1), (4) MZ/2GO-Cu (GC2) composites by the disk-diffusion test against both gram-positive (*S. aureus*) and gram-negative (*E. coli*), (**b**) plate count technique results of the MZ, MZ/GO and MZ/1GO-Cu composites. Note: (1): MZ, (2): MZ/GO, (3): MZ/1GO-Cu, (4): MZ/2GO-Cu (* $p < 0.05$).

Gram-positive bacteria have a single cytoplasmic membrane that is multilayered with peptidoglycan polymer [39,40], as well as a comparatively thick cell wall of about 20 to 80 nm. In contrast, the wall of gram-negative bacteria is made up of two cell membranes: an outer membrane and a plasma membrane with a thin layer of peptidoglycan that is 7 to 8 nm thick [39,40]. The structural and compositional variations between gram-positive and gram-negative bacteria may explain the MZ/GO-Cu coating's superior antibacterial effectiveness against gram-positive bacteria.

Colonies of *E. coli* and *S. aureus* bacteria on the surface of the MZ/GO-Cu composites and the control sample incubated for 24 h are shown in Figure 10b. A significant number of colonies of *E. coli* and *S. aureus* bacteria can be found on the control sample, showing a lack of antibacterial activity in this specimen. On the other hand, no bacterial colony, such as *E. coli* and *S. aureus* bacteria, can be detected on the MZ/GO-Cu composite, showing that the MZ/GO-Cu composite has a good antibacterial property. Cu is required by microorganisms, including bacteria, at low concentrations as an important micronutrient, but at high concentrations, Cu can prevent cell growth or even trigger cell death. In this regard, it was reported [39] that for solid Cu alloy, the antibacterial efficacy of Cu-based alloys against Salmonella choleraesuis improved as the Cu content increased.

MZ composite with high Cu-GO content has significant antibacterial activity. MZ/GO-Cu composites against *S. aureus* had a similar reduction rate, with between 90 and 94% of bacteria being destroyed. In contrast to other samples (MZ alloy and MZ/GO composites), the GC2 composite had a significantly higher bacterial inhibition rate. A possible reason for the antibacterial properties of MZ/GO-Cu composites is the Cu-GO nanosystem's synergistic antibacterial activity. GO, with a sheet-like structure has several unique properties, such as having a high specific surface area, having a large number of oxygen-containing functional groups on the surface, being negatively charged, having a large-conjugated structure, and so on, that allow it to hydrogen bond with bacterial cellular membrane components such as lipids and proteins [40]. GO nanosheets can adsorb onto bacterial cells, wrap around them, and trap them as a result of the interaction. The sharp edges of GO nanosheets have been shown to infiltrate and damage bacterial cytomembranes [41–45]. When Cu nanoparticles were loaded on GO nanosheets, the absorbing, wrapping, and capturing effects of the GO nanosheets could increase the local concentration of Cu nanoparticles around the bacterial cells, exposing the bacteria to more antibacterial action [5,42]. Cu nanoparticles' antibacterial activity was mostly based on the release of Cu and the promotion of reactive oxygen species (ROS). Cu was formed by oxidizing Ag with oxygen and water [2,20], while ROS is produced by catalyzing the single electron reduction of O_2 with Cu or by impairing bacteria's respiratory chains [30]. Highly reactive Cu and ROS may damage several bacterial cellular structures and functions [24], such as attacking the cytomembrane and disrupting transmembrane transport, attacking respiratory enzyme and inhibiting ATP synthesis, attacking DNA and inhibiting replication and transcription, attacking mRNA and disrupting transcription, and attacking protein [22]. To summarize, the synergistic antibacterial activity of GO and Cu may be attributed to the GO nanosheets' capturing effects and the Cu nanoparticles' killing effects.

4. Conclusions

In the present study, the potential for enhancing the mechanical and antibacterial properties of Mg-Zn (MZ) alloy by the addition of GO-Cu nanoreinforcement membranes was extensively explored. GO-Cu nanoreinforcement can enhance the mechanical and antibacterial properties of the Mg-based matrix in a synergistic route. The compressive strength of the MZ/2GO-Cu composite was increased to 200 $\pm$ 6 MPa. Grain refining, precipitate strengthening and dispersion strengthening contributed to the increase in compressive strength. Meanwhile, due to Cu-GO's superior antibacterial properties, the diameters of the MZ/GO-Cu composite inhibition zones against *E. coli* and *S. aureus* are increased by 3.64 mm and 4.03 mm, respectively. However, the MZ/GO composite encapsulated with Cu alloys presented a higher degradation rate in SBF compared to MZ

alloy and MZ/GO composite. Furthermore, cell culture studies indicated that the MZ/GO-Cu composite with a low concentration of GO-Cu was cytocompatible. GO-Cu integration has much promise for enhancing both the mechanical and antibacterial performance of the MZ/GO-Cu composite for biomedical applications.

Author Contributions: Conceptualization, supervision, formal analysis, writing—review and editing, H.R.B.-R.; writing—original draft preparation, formal analysis, A.S. and M.R.; conceptualization, writing—review and editing, A.F.I., S.S., and S.R.; conceptualization, writing—review and editing, funding acquisition, F.B. All authors have read and agreed to the published version of the manuscript.

Funding: This research received no external funding.

Institutional Review Board Statement: Not applicable.

Informed Consent Statement: Not applicable.

Data Availability Statement: All data provided in the present manuscript are available to whom it may concern.

Conflicts of Interest: The authors declare that they have no competing/financial conflict of interest.

References

1. Cui, Z.; Li, W.; Cheng, L.; Gong, D.; Cheng, W.; Wang, W. Effect of nano-HA content on the mechanical properties, degradation and biocompatible behavior of Mg-Zn/HA composite prepared by spark plasma sintering. *Mater. Charact.* **2019**, *151*, 620–631. [CrossRef]
2. Liao, J.; Hotta, M.; Motoda, S.-I.; Shinohara, T. Atmospheric corrosion of two field-exposed AZ31B magnesium alloys with different grain size. *Corros. Sci.* **2013**, *71*, 53–61. [CrossRef]
3. Liao, J.; Hotta, M.; Yamamoto, N. Corrosion behavior of fine-grained AZ31B magnesium alloy. *Corros. Sci.* **2012**, *61*, 208–214. [CrossRef]
4. Shuai, C.; Guo, W.; Wu, P.; Yang, W.; Hu, S.; Xia, Y.; Feng, P. A graphene oxide-Ag co-dispersing nanosystem: Dual synergistic effects on antibacterial activities and mechanical properties of polymer scaffolds. *Chem. Eng. J.* **2018**, *347*, 322–333. [CrossRef]
5. Lin, Z.; Sun, X.; Yang, H. The Role of Antibacterial Metallic Elements in Simultaneously Improving the Corrosion Resistance and Antibacterial Activity of Magnesium Alloys. *Mater. Des.* **2021**, *198*, 109350. [CrossRef]
6. Saberi, A.; Bakhsheshi-Rad, H.; Karamian, E.; Kasiri-Asgarani, M.; Ghomi, H. Magnesium-graphene nano-platelet composites: Corrosion behavior, mechanical and biological properties. *J. Alloys Compd.* **2020**, *821*, 153379. [CrossRef]
7. Ali, M.; Hussein, M.; Al-Aqeeli, N. Magnesium-based composites and alloys for medical applications: A review of mechanical and corrosion properties. *J. Alloys Compd.* **2019**, *792*, 1162–1190. [CrossRef]
8. Hassan, S.F.; Islam, M.T.; Nouari, S.; Baig, M.M.A.; Patel, F.; Al-Aqeeli, N. Extraordinary Strengthening of Magnesium by Solid-State Diffusion of Copper in Mg-0.5Cu Alloy. *JOM* **2020**, *72*, 1597–1606. [CrossRef]
9. Jayalakshmi, S.; Sankaranarayanan, S.; Singh, R.A.; Shabadi, R.; Gupta, M. Utilizing Iron as Reinforcement to Enhance Ambient Mechanical Response and Impression Creep Response of Magnesium. *Metals* **2021**, *11*, 1448. [CrossRef]
10. Dutta, S.; Gupta, S.; Roy, M. Recent Developments in Magnesium Metal–Matrix Composites for Biomedical Applications: A Review. *ACS Biomater. Sci. Eng.* **2020**, *6*, 4748–4773. [CrossRef]
11. Yamada, R.; Yoshihara, S.; Ito, Y. Fatigue Properties of AZ31B Magnesium Alloy Processed by Equal-Channel Angular Pressing. *Metals* **2021**, *11*, 1191. [CrossRef]
12. Sripathy, A.P.; Handjaja, C.; Manakari, V.; Parande, G.; Gupta, M. Development of Lightweight Magnesium/Glass Micro Balloon Syntactic Foams Using Microwave Approach with Superior Thermal and Mechanical Properties. *Metals* **2021**, *11*, 827. [CrossRef]
13. Sharma, A.; Kopylov, A.; Zadorozhnyy, M.; Stepashkin, A.; Kudelkina, V.; Wang, J.-Q.; Ketov, S.; Churyukanova, M.; Louzguine-Luzgin, D.; Sarac, B.; et al. Mg-Based Metallic Glass-Polymer Composites: Investigation of Structure, Thermal Properties, and Biocompatibility. *Metals* **2020**, *10*, 867. [CrossRef]
14. González-Murguía, J.L.; Veleva, L.; Rodríguez-Gattorno, G.; Figueroa-Torres, M.Z.; Feliu, S. Mg-Ca0.3 Electrochemical Activity Exposed to Hank's Physiological Solution and Properties of Ag-Nano-Particles Deposits. *Metals* **2021**, *11*, 1357. [CrossRef]
15. Dobrzański, L.A.; Totten, G.E.; Bamberger, M. (Eds.) *Magnesium and Its Alloys: Technology and Applications*, 1st ed.; CRC Press: Boca Raton, FL, USA, 2019. [CrossRef]
16. Dobrzański, L.A.; Totten, G.E.; Bamberger, M. The Importance of Magnesium and Its Alloys in Modern Technology and Methods of Shaping Their Structure and Properties. In *Magnesium and Its Alloys*; CRC Press: Boca Raton, FL, USA, 2019; pp. 1–28.
17. Metalnikov, P.; Ben-Hamu, G.; Shin, K.; Eliezer, A. Effect of Ca Addition on Corrosion Behavior of Wrought AM60 Magnesium Alloy in Alkaline Solutions. *Metals* **2021**, *11*, 1172. [CrossRef]
18. Emelyanenko, A.; Kaminsky, V.; Pytskii, I.; Emelyanenko, K.; Domantovsky, A.; Chulkova, E.; Shiryaev, A.; Aleshkin, A.; Boinovich, L. Antimicrobial Activity and Degradation of Superhydrophobic Magnesium Substrates in Bacterial Media. *Metals* **2021**, *11*, 1100. [CrossRef]

19. Güler, Ö.; Bağcı, N. A short review on mechanical properties of graphene reinforced metal matrix composites. *J. Mater. Res. Technol.* **2020**, *9*, 6808–6833. [CrossRef]
20. Bakhsheshi-Rad, H.R.; Ismail, A.F.; Aziz, M.; Akbari, M.; Hadisi, Z.; Khoshnava, S.M.; Pagan, E.; Chen, X. Co-incorporation of graphene oxide/silver nanoparticle into poly-L-lactic acid fibrous: A route toward the development of cytocompatible and antibacterial coating layer on magnesium implants. *Mater. Sci. Eng. C* **2020**, *111*, 110812. [CrossRef]
21. Shuai, C.; Liu, L.; Zhao, M.; Feng, P.; Yang, Y.; Guo, W.; Gao, C.; Yuan, F. Microstructure, biodegradation, antibacterial and mechanical properties of ZK60-Cu alloys prepared by selective laser melting technique. *J. Mater. Sci. Technol.* **2018**, *34*, 1944–1952. [CrossRef]
22. Liu, C.; Fu, X.; Pan, H.; Wan, P.; Wang, L.; Tan, L.; Wang, K.; Zhao, Y.; Yang, K.; Chu, P. Biodegradable Mg-Cu alloys with enhanced osteogenesis, angiogenesis, and long-lasting antibacterial effects. *Sci. Rep.* **2016**, *6*, 27374. [CrossRef]
23. Xu, R.; Zhao, M.-C.; Zhao, Y.-C.; Liu, L.; Liu, C.; Gao, C.; Shuai, C.; Atrens, A. Improved biodegradation resistance by grain refinement of novel antibacterial ZK30-Cu alloys produced via selective laser melting. *Mater. Lett.* **2019**, *237*, 253–257. [CrossRef]
24. Li, Y.; Liu, L.; Wan, P.; Zhai, Z.; Mao, Z.; Ouyang, Z.; Yu, D.; Sun, Q.; Tan, L.; Ren, L.; et al. Biodegradable Mg-Cu alloy implants with antibacterial activity for the treatment of osteomyelitis: In vitro and in vivo evaluations. *Biomaterials* **2016**, *106*, 250–263. [CrossRef] [PubMed]
25. Tao, J.-X.; Zhao, M.-C.; Zhao, Y.-C.; Yin, D.-F.; Liu, L.; Gao, C.; Shuai, C.; Atrens, A. Influence of graphene oxide (GO) on microstructure and biodegradation of ZK30-xGO composites prepared by selective laser melting. *J. Magnes. Alloy.* **2020**, *8*, 952–962. [CrossRef]
26. Cai, N.; Zeng, H.; Fu, J.; Chan, V.; Chen, M.; Li, H.; Yu, F. Synergistic effect of graphene oxide-silver nanofillers on engineering performances of polyelectrolyte complex nanofiber membranes. *J. Appl. Polym. Sci.* **2018**, *135*, 46238. [CrossRef]
27. Munir, K.S.; Wen, C.; Li, Y. Carbon Nanotubes and Graphene as Nanoreinforcements in Metallic Biomaterials: A Review. *Adv. Biosyst.* **2019**, *3*, e1800212. [CrossRef] [PubMed]
28. Shuai, C.; Wang, B.; Bin, S.; Peng, S.; Gao, C. Interfacial strengthening by reduced graphene oxide coated with MgO in biodegradable Mg composites. *Mater. Des.* **2020**, *191*, 108612. [CrossRef]
29. Askarnia, R.; Fardi, S.R.; Sobhani, M.; Staji, H. Ternary hydroxyapatite/chitosan/graphene oxide composite coating on AZ91D magnesium alloy by electrophoretic deposition. *Ceram. Int.* **2021**, *47*, 27071–27081. [CrossRef]
30. Gao, C.; Feng, P.; Peng, S.; Shuai, C. Carbon nanotube, graphene and boron nitride nanotube reinforced bioactive ceramics for bone repair. *Acta Biomater.* **2017**, *61*, 1–20. [CrossRef]
31. Dezfuli, S.N.; Huan, Z.; Mol, A.; Leeflang, S.; Chang, J.; Zhou, J. Advanced bredigite-containing magnesium-matrix composites for biodegradable bone implant applications. *Mater. Sci. Eng. C* **2017**, *79*, 647–660. [CrossRef] [PubMed]
32. Song, X.; Bayati, P.; Gupta, M.; Elahinia, M.; Haghshenas, M. Fracture of magnesium matrix nanocomposites—A review. *Int. J. Light. Mater. Manuf.* **2021**, *4*, 67–98. [CrossRef]
33. Shahin, M.; Munir, K.; Wen, C.; Li, Y. Magnesium-based composites reinforced with graphene nanoplatelets as biodegradable implant materials. *J. Alloys Compd.* **2020**, *828*, 154461. [CrossRef]
34. Shuai, C.; Wang, B.; Yang, Y.; Peng, S.; Gao, C. 3D honeycomb nanostructure-encapsulated magnesium alloys with superior corrosion resistance and mechanical properties. *Compos. Part B:Eng.* **2019**, *162*, 611–620. [CrossRef]
35. Zheng, Y.F.; Gu, X.N.; Witte, F. Biodegradable metals. *Mater. Sci. Eng. R Rep.* **2014**, *77*, 1–34. [CrossRef]
36. Kim, J.D.; Yun, H.; Kim, G.C.; Lee, C.W.; Choi, H.C. Antibacterial activity and reusability of CNT-Ag and GO-Ag nanocomposites. *Appl. Surf. Sci.* **2013**, *283*, 227–233. [CrossRef]
37. Depan, D.; Girase, B.; Shah, J.S.; Misra, R.D.K. Structure–process–property relationship of the polar graphene oxide-mediated cellular response and stimulated growth of osteoblasts on hybrid chitosan network structure nanocomposite scaffolds. *Acta Biomater.* **2011**, *7*, 3432–3445. [CrossRef] [PubMed]
38. Shuai, C.; Wang, B.; Bin, S.; Peng, S.; Gao, C. TiO2-Induced In Situ Reaction in Graphene Oxide-Reinforced AZ61 Biocomposites to Enhance the Interfacial Bonding. *ACS Appl. Mater. Interfaces* **2020**, *12*, 23464–23473. [CrossRef]
39. Sirelkhatim, A.; Mahmud, S.; Seeni, A.; Kaus, N.H.M.; Ann, L.C.; Bakhori, S.K.M.; Hasan, H.; Mohamad, D. Review on Zinc Oxide Nanoparticles: Antibacterial Activity and Toxicity Mechanism. *Nano-Micro Lett.* **2015**, *7*, 219–242. [CrossRef]
40. Fu, G.; Vary, A.P.S.; Lin, C.-T. Anatase TiO2 Nanocomposites for Antimicrobial Coatings. *J. Phys. Chem. B* **2005**, *109*, 8889–8898. [CrossRef]
41. Singh, A.; Dubey, A.K. Various Biomaterials and Techniques for Improving Antibacterial Response. *ACS Appl. Bio Mater.* **2018**, *1*, 3–20. [CrossRef]
42. Hegab, H.M.; ElMekawy, A.; Zou, L.; Mulcahy, D.; Saint, C.; Ginic-Markovic, M. The controversial antibacterial activity of graphene-based materials. *Carbon* **2016**, *105*, 362–376. [CrossRef]
43. Cabeza, S.; Pérez Zubiaur, P.; Garcés, G.; Andrade, C.; Adeva, P. Corrosion Behaviour of Mg98.5Nd1Zn0.5 (at. %) Alloy in Phosphate Buffered Saline Solution. *Metals* **2020**, *10*, 148. [CrossRef]
44. Dizaj, S.M.; Lotfipour, F.; Barzegar-Jalali, M.; Zarrintan, M.H.; Adibkia, K. Antimicrobial activity of the metals and metal oxide nanoparticles. *Mater. Sci. Eng. C* **2014**, *44*, 278–284. [CrossRef] [PubMed]
45. Yousefi, M.; Dadashpour, M.; Hejazi, M.; Hasanzadeh, M.; Behnam, B.; de la Guardia, M.; Shadjou, N.; Mokhtarzadeh, A. Anti-bacterial activity of graphene oxide as a new weapon nanomaterial to combat multidrug-resistance bacteria. *Mater. Sci. Eng. C* **2017**, *74*, 568–581. [CrossRef] [PubMed]